Published on 25 September 2020. Downloaded by Indian Institute of Science on 12/30/2021 11:43:08 AM.

Sustainable Energy & Fuels

ROYAL SOCIETY OF CHEMISTRY

PAPER

View Article Online
View Journal | View Issue

Check for updates

Cite this: *Sustainable Energy Fuels*, 2020, 4, 5721

Molecular insights into photostability of fluorinated organic photovoltaic blends: role of fullerene electron affinity and donor–acceptor miscibility†

Colin P. Brook, [a] Goutam Paul,[b] Vinila Nellissery Viswanathan,[c] Sandeep Satyanarayana,[c] Kumar M. Panidhara,[c] Bryon W. Larson, [d] Andrew J. Ferguson, [d] Amlan J. Pal, [b] Praveen C. Ramamurthy,[c] Steven H. Strauss, [a] Olga V. Boltalina [a] and Wade A. Braunecker [*d]

Received 3rd July 2020
Accepted 18th September 2020

DOI: 10.1039/d0se00971g

rsc.li/sustainable-energy

In this work, the photostability of certain organic photovoltaic (OPV) active layers was demonstrated to improve by as much as a factor of five under white light illumination in air with the use of 1,7-bis-trifluoromethylfullerene ($C_{60}(CF_3)_2$) as the acceptor in place of $PC_{60}BM$. However, the results were highly dependent on the structure and functionality within the donor material. Twelve combinations of active layer blends were studied, comprised of six different high-performance donor polymers (two fluorinated and four non-fluorinated donors) and two fullerene acceptors ($PC_{60}BM$ and $C_{60}(CF_3)_2$). The relative rates of irreversible photobleaching of the active layer blends were found to correlate well with the electron affinity of the fullerene when the polymer and fullerene were well blended, but a full rationalization of the photobleaching data requires consideration of both the electron affinity of the fullerene as well as the relative miscibility of the polymer–fullerene components in the blend. Miscibility of those components was probed using a combination of time-resolved photoluminescence (TRPL) measurements and scanning tunneling microscopy (STM) imaging. The presence of fluorinated aromatic units in the donor materials tend to promote more intimate mixing with $C_{60}(CF_3)_2$ as compared to $PC_{60}BM$. The full results of these photobleaching studies and measurements of donor–acceptor miscibility, considered alongside additional photoconductance measurements and preliminary device work, provide new molecular optimization insights for improving the long-term stability of OPV active layers.

1. Introduction

The potential for organic photovoltaics (OPVs) to offer an inexpensive source of renewable energy in the form of light-weight and flexible modules[1,2] has been driving extensive research efforts in the field.[3–5] With reports of single junction[6,7] and tandem cells[8] now exceeding 17% power conversion efficiencies (PCEs), along with recent advances in large area printing of OPV modules,[1,9] the technology is becoming increasingly commercially viable. However, while encapsulation of the active layer can extend the operational lifetimes of certain OPV systems from days to years,[10,11] the intrinsic instability of the active layer remains a pertinent obstacle to the wide-spread real-world application of OPV technology.[9,10,12] While there are multiple known pathways that contribute to degradation,[12–15] thermal instability of the active layer morphology and irreversible photobleaching of the active layer components are typically the most detrimental.

The most favorable active layer architecture in high performance devices is the bulk heterojunction (BHJ), which exists as a metastable state consisting of interpenetrating domains of an electron donating material (typically a small molecule or conjugated polymer) and an electron accepting material (typically a fullerene derivative, although efficient non-fullerene acceptors are becoming more common[5]). The BHJ architecture both maximizes the amount of donor–acceptor contact for charge generation and separation, while producing morphologies that facilitate charge transport to the electrodes.[16] However, because it is a metastable state, the BHJ is intrinsically susceptible to degradation under operating conditions through phase separation over time. While less common, some blends

[a]Department of Chemistry, Colorado State University, Fort Collins, Colorado 80523, USA

[b]School of Physical Sciences, Indian Association for the Cultivation of Science, Jadavpur, Kolkata 700032, India

[c]Department of Materials Engineering, Indian Institute of Science, Bangalore, Karnataka, 560012, India

[d]National Renewable Energy Laboratory, 15013 Denver West Parkway, Golden, Colorado 80401, USA. E-mail: Wade.Braunecker@nrel.gov

† Electronic supplementary information (ESI) available: Polymer characterization, experimental details regarding film preparation, STM/STS analysis, TRPL and TRMC measurements, and OPV device work. See DOI: 10.1039/d0se00971g

Published on 25 September 2020. Downloaded by Indian Institute of Science on 12/30/2021 11:43:08 AM.

containing very crystalline polymers have even been observed to phase separate at room temperature when kept in the dark.[17] In principle, improving the general miscibility between the donor and acceptor should help prevent phase separation, thereby improving the thermal stability of the active layer morphology by corollary.[18] In fact, several recent studies have demonstrated correlations between polymer–fullerene miscibility and critical device metrics such as improved charge collection efficiency[19] and fill factor.[20] Furthermore, by understanding temperature-dependent miscibility, the stability and mixing behaviors of certain components of polymer solar cells have been optimized at processing and operating temperatures.[21]

Perhaps more detrimental than phase separation to device performance is exposure of the active layer to light in the presence of oxygen. This can cause the donor polymer to undergo complete irreversible photobleaching within several minutes to a few days if the active layer is not encapsulated.[22] While encapsulation with various materials is quite effective at slowing (though not eliminating) oxygen and moisture permeation to the active layer,[11] the anti-fouling properties, adhesion, and the ability of PV polymeric encapsulants to preclude moisture and oxygen can also degrade over time.[23] Thus, any improvements to the intrinsic photo-oxidative stability of the OPV active layer would help extend the useful lifetime of a working device.

Currently, the primary mechanism involved in photobleaching of the donor polymer in the presence of oxygen is believed to proceed *via* a radical pathway.[24] It has been proposed that both the polymer and fullerene can donate photogenerated electrons to diatomic oxygen to form a superoxide radical anion, and that the radical anion is in turn responsible for degrading the polymer. Moreover, it has been shown that there is a strong inverse correlation between the electron affinity (EA) of the fullerene acceptor and the rate of photobleaching of the donor polymer in BHJ blends.[22] In a series of five fullerenes with EAs ranging from 3.77 eV to 4.07 eV, $PC_{60}BM$ had the largest EA and demonstrated the greatest stabilizing effect, regardless of the donor polymer tested. The results implied that the larger the EA of the fullerene, that is the deeper its lowest unoccupied molecular orbital (LUMO), the more stable the polymer donor in the blend became towards photo-oxidation.

Trifluoromethylfullerenes (TMFs) are typically more intrinsically photo-oxidatively and thermally stable than $PC_{60}BM$, which can degrade over time into $PC_{60}BM$-oxide.[25,26] The LUMO energies tend to be much deeper than $PC_{60}BM$ and are tunable through $-CF_3$ additions, suggesting they are promising materials for improving the stability of the donor polymer in OPV blends. The simplest and most electropositive TMF, $C_{60}(CF_3)_2$, has a LUMO energy *ca.* 220 meV deeper than $PC_{60}BM$.[27] Indeed, we recently observed that $C_{60}(CF_3)_2$ could stabilize the initial rate of photobleaching in small molecule and polymer blends by a factor of 15 relative to $PC_{70}BM$.[28] However, phase-separation of $C_{60}(CF_3)_2$ from the small molecule donor material was observed that resulted in dramatic acceleration of the photobleaching rate in less than 24 h of white light exposure. Those results suggest that if there is a substantial difference in miscibility between different fullerenes and a given donor material, the EA of the fullerene alone will not be the only factor determining its stabilizing effect.[29] Additionally, while many TMFs are known to be highly crystalline materials,[30] recent work has demonstrated that polymer–fullerene miscibility has more influential effects than the crystallinity of single components on certain optimization parameters in polymer–fullerene solar cells.[31] Indeed, the miscibility of several high performance donor–acceptor combinations has been correlated with improved device performance.[19,32,33] The results suggest that understanding and improving the miscibility of TMFs with common high performance donor materials or their derivatives could be an effective strategy for improving the intrinsic stability of the active layer, as well as the overall efficiency of devices.

Incidentally, fluorinated donor polymers have received notable interest as components of high performance OPV active layers.[5,34–38] Fluorine substitution into the polymer backbone has been shown to impart a number of beneficial effects on the material as an OPV donor: strategic fluorination can (i) increase polymer crystallinity,[39] which in turn can improve both charge mobility[40] and photostability;[41] (ii) tune the optoelectronic properties of the donor material;[42] and (iii) strongly influence dipole moments in the material that in turn affect charge separation and recombination.[43] Specific fluorine interactions can also have a strong influence on the solid-state morphology of active layer blends,[4,38,44–46] and they have recently been employed by our group to influence long-range structural order in other organic conjugated systems such as covalent organic frameworks.[47]

For this work, we focused our efforts on several high performance OPV polymers and their structural analogues, shown in Fig. 1. Copolymers based on thienopyrrolodione (TPD) have been widely studied with a variety of electron rich comonomers, most notably derivatives of benzodithiophene (BDT),[48] but also comonomers such as cyclopentadithiophene (CPDT).[49] Depending on the side chains, TPD-BDT copolymers have been optimized above 8.5% PCE with conventional device structures[50] and TPD-CPDT above 6%.[49] TPD-BDT polymers are known to be some of the most photo-oxidatively stable copolymers that simultaneously display high OPV efficiencies, while also being widely commercially available. The polymer commercially known as PCE11 (shown in Fig. 1, see ESI† for full name) and its analogues have displayed optimized efficiencies near 11%,[51] and we reasoned that the fluorinated aromatic units in the backbone may serve to improve miscibility with our fluorinated fullerene through well-known phenyl–perfluorophenyl stacking interactions.[47] Polymer donors that were structurally related to PCE11 were also synthesized by combining either the fluorinated or non-fluorinated benzothiadiazole (BT) unit with the BDT comonomer. A wide-variety of these BT-BDT materials have been synthesized in the literature, with many of the materials exceeding 5–6% efficiency.[52]

Herein, case studies investigating several combinations of fluorinated and non-fluorinated high-performance donor polymers with both $PC_{60}BM$ and $C_{60}(CF_3)_2$ are presented. The miscibility of the components was probed using time-resolved

Published on 25 September 2020. Downloaded by Indian Institute of Science on 12/30/2021 11:43:08 AM.

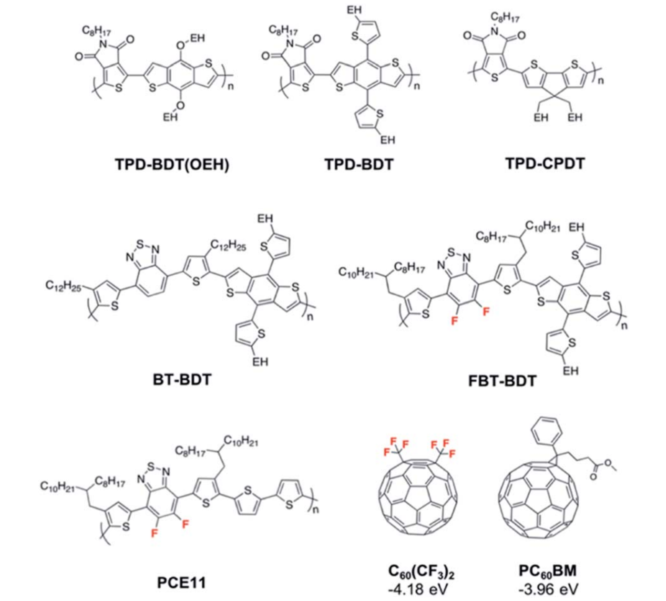

Fig. 1 Chemical structure of polymers and fullerenes used in this study. Fluorine atoms are labeled in red for clarity. LUMO energies were calculated from CV data: LUMO $= -((E_{1/2}{}^{0/-}$ *vs.* $Fe(Cp)_2{}^{+/0}) + 5.1)$ eV, where $C_{60}{}^{0/-} = 1.05$ (eV) *vs.* $Fe(Cp)_2{}^{+/0}$. $E_{1/2}{}^{0/-}$ values are taken from the literature of CVs performed in *o*-DCB[27] with $Fe(Cp)_2{}^{+/0}$ as an internal reference. See ESI† for synthesis or source of materials. EH denotes branched ethyl-hexyl side chains.

photoluminescence (TRPL) and scanning tunneling microscopy (STM). Those results and the fullerene's respective EA were correlated with the overall photo-oxidative stability of the active layer, and finally, the intrinsic photoconductance of the active layer material.

2. Results and discussion

2.1. Photobleaching

For each polymer and fullerene used in this study, non-encapsulated films of neat polymer and blends of 1 : 1 by mass of polymer–fullerene were aged in air under a quad array of tungsten halogen lamps with intensity ~0.7 suns (70 mW cm^{-2}). The surface temperature of the substrates under the lamp was recorded as 60 °C. The spin coating procedures were optimized for each blend (recorded in the ESI†) such that each film had an initial absorbance of *ca.* 0.3 absorbance units at the red-edge λ_{max} (Fig. S2†). Absorbance spectra were measured periodically over the course of several weeks (see Fig. 2 for a representative example).

Absorbance data at the red-edge λ_{max} for each film was used to evaluate the time required to bleach each film to 80% and then 60% of its initial absorbance (T_{80} and T_{60}, respectively). The results were repeated in triplicate, with average degradation lifetimes recorded in Table 1. The overall decrease in the absorbance spectrum, and for some polymers the blue shift in λ_{max}, is consistent with the loss of conjugation in the polymer backbone that occurs during photodegradation of the material.[24]

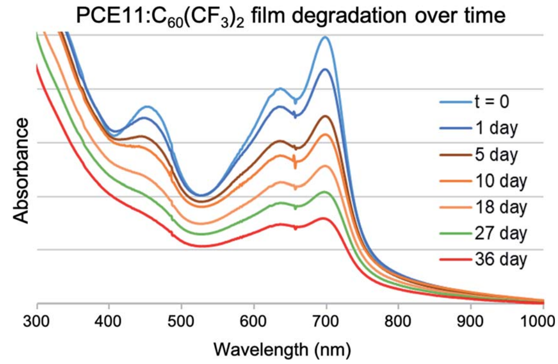

Fig. 2 Representative example of UV-vis absorbance spectra collected during photobleaching experiments for 1 : 1 by weight blend of PCE11–$C_{60}(CF_3)_2$.

Before discussing important nuances in the photobleaching data, the following general observations were made about the results recorded in Table 1. First, in all twelve blends, the addition of a fullerene to the polymer resulted in improved stability over the neat polymer system. Second, the apparent rates of degradation can change dramatically between the T_{80} and T_{60}, either apparently stabilizing or accelerating depending on a given sample (*vide infra*). Indeed, recent literature results have shown that phase separation of the polymer and fullerene can happen with time; this phenomenon has been independently observed both with blends of $C_{60}(CF_3)_2$ (ref. 28) and in systems with PCE11.[17] Finally, in some cases the fluorinated fullerene acts as a more efficient stabilizer of the polymer towards photodegradation, and in other cases $PC_{60}BM$ is more efficient. We now discuss these nuances in more detail, first for the TPD-based polymers.

The bleaching behavior of the three TPD-based polymers (–BDT(OEH), –BDT, and –CPDT, entries 1–3 in Table 1) is shown in the top of Fig. 3 and compares the decrease in fraction of light absorbed (FA) over time. The behavior varied significantly from one system to another for both the neat samples and the blends. For example, with regards to the neat polymer films, the TPD-CPDT bleached approximately one order of magnitude faster than both TPD-BDT-based polymers. Though we cannot say conclusively why the CPDT unit is intrinsically less stable, the α-hydrogens on the side chains of conjugated OPV monomers are known to be particularly susceptible to degradation by free radical abstraction,[22] and such α-hydrogens are not present in either BDT monomer unit like they are in CPDT. Regarding the blends, there was a marked difference in the stabilizing effects of the two fullerenes amongst these TPD-polymers. For example, the TPD-CPDT blend with $C_{60}(CF_3)_2$ was five times more stable than a blend with $PC_{60}BM$ (determined from T_{80}), as might be anticipated from the lower lying LUMO of the fluorinated fullerene based on all the aforementioned observed trends. However, the TPD-BDT blend with $C_{60}(CF_3)_2$ was only marginally more stable towards photodegradation than a blend with $PC_{60}BM$, with a T_{80} of 46 h *vs.* 41 h with $PC_{60}BM$; for the TPD-BDT(OEH) blends, the trend was actually inverted, with $PC_{60}BM$ being a more effective stabilizer than $C_{60}(CF_3)_2$. Based

Published on 25 September 2020. Downloaded by Indian Institute of Science on 12/30/2021 11:43:08 AM.

Table 1 Lifetime of neat and blended films aged in air

Polymer	Blend	T_{80} (h)	Relative[a] T_{80}	T_{60} (h)	Relative[a] T_{60}
TPD-BDT(OEH)	Neat	19	—	58	—
	$PC_{60}BM$	86	4.5	288	5.0
	$C_{60}(CF_3)_2$	60	3.2	192	3.3
TPD-BDT	Neat	16	—	65	—
	$PC_{60}BM$	41	2.6	106	1.6
	$C_{60}(CF_3)_2$	46	2.9	137	2.1
TPD-CPDT	Neat	1.6	—	6.6	—
	$PC_{60}BM$	2.2	1.4	7.7	1.2
	$C_{60}(CF_3)_2$	11	6.9	28	4.2
PCE11	Neat	53	—	91	—
	$PC_{60}BM$	72	1.4	173	1.9
	$C_{60}(CF_3)_2$	91	1.7	360	4.0
FBT-BDT	Neat	9.6	—	21	—
	$PC_{60}BM$	20	2.1	58	2.8
	$C_{60}(CF_3)_2$	58	6.0	161	7.7
BT-BDT	Neat $PC_{60}BM$	17	—	67	—
	$C_{60}(CF_3)_2$	163	9.6	648	9.7
		108	6.4	624	9.3

[a] Relative values of T_{80} and T_{60} for a given blend were calculated by normalizing them to the T_{80} and T_{60} values for their respective neat polymer film. See Fig. S3 and S4 in the ESI for graphical representation of T_{80} and T_{60} values.

on this observation, we hypothesized that the TPD-BDT(OEH) may not be as miscible with $C_{60}(CF_3)_2$ as it is with $PC_{60}BM$, which we investigate and discuss in more detail in subsequent sections.

When comparing the bleaching behavior of BT-based materials over time, shown in the bottom of Fig. 3, perhaps the most important observation was that for both fluorinated donors (FBT-BDT and PCE11), $C_{60}(CF_3)_2$ was a more efficient

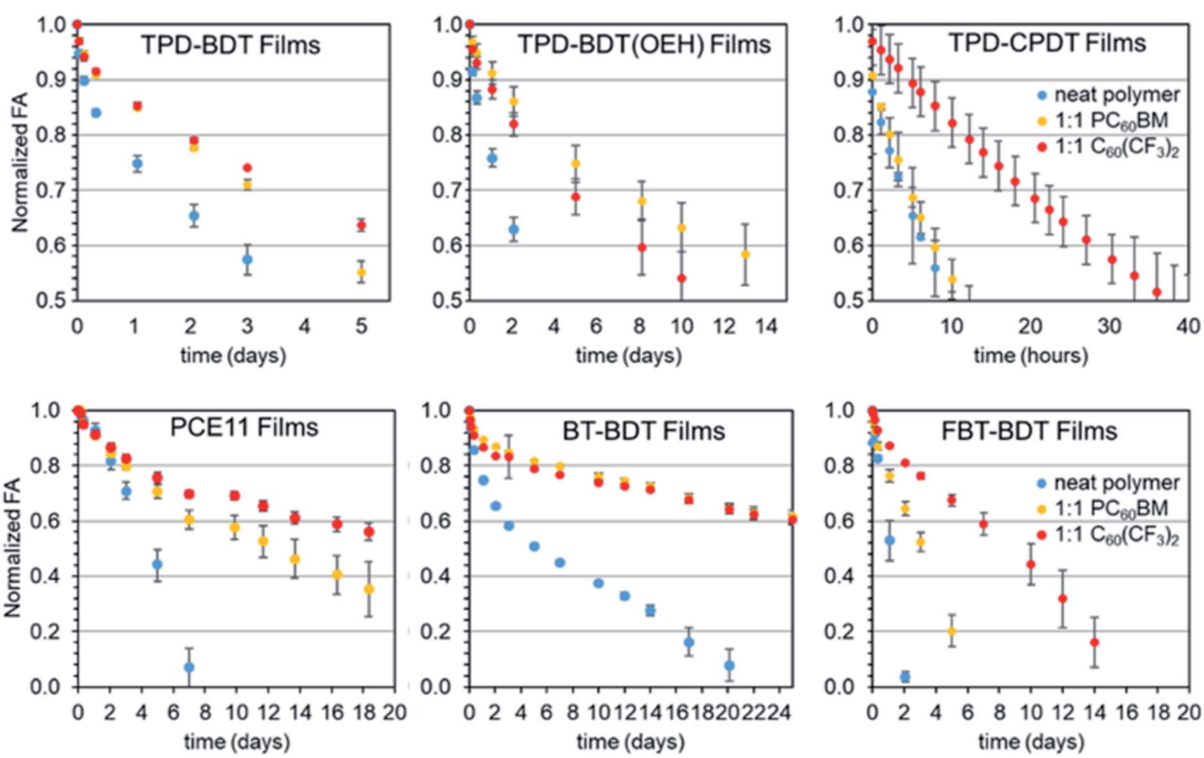

Fig. 3 Fraction of light absorbed over time measured at λ_{max} for films of neat polymer and fullerene blends containing TPD-BDT, TPD-BDT(OEH) and TPD-CPDT (top left to top right), and PCE11, BT-BDT, and FBT-BDT (bottom left to right). Inset in the right most graph shows color key for each film type. All neat films are represented in blue. 1 : 1 (by mass) blends of polymer with $PC_{60}BM$ and $C_{60}(CF_3)_2$ are orange and red, respectively. Note, the x-axes are not at the same scale; each figure shows degradation up to the T_{60} values for the most stable fullerene blend for that given polymer.

 This journal is © The Royal Society of Chemistry 2020

Published on 25 September 2020. Downloaded by Indian Institute of Science on 12/30/2021 11:43:08 AM.

stabilizer of the polymer towards photodegradation than $PC_{60}BM$ by a factor of two to three, whereas all the other polymers investigated (with the exception of TPD-CPDT) saw either no or only a small improvement in the photostability with $C_{60}(CF_3)_2$ relative to $PC_{60}BM$. Furthermore, the relative rate of photobleaching of PCE11 in the $PC_{60}BM$ blend appeared to increase over time relative to the $C_{60}(CF_3)_2$ blend when we compare T_{60} and T_{80} values in Table 1 (or look at Fig. 3 which shows how the photobleaching dynamics for PCE11 films change past the T_{60} value). Indeed PCE11 is known to phase separate with time from $PC_{60}BM$ even when kept in the dark as a result of thermally driven phase separation.[17] These results suggest the PCE11–$C_{60}(CF_3)_2$ system may remain more intimately blended relative to $PC_{60}BM$. For the non-fluorinated BT-BDT polymer, the opposite trend was true; the $PC_{60}BM$ blend was *slightly* more stable than that with the $C_{60}(CF_3)_2$, although both had significant stabilizing effects.

Overall, the bleaching behavior in these blends is complex and cannot be simply rationalized based solely on the relative electron affinity of the two fullerenes. In reality, it is difficult to disentangle the effects of photo and thermal stability of the blends, as we have previously observed that small amounts of photo-induced degradation of OPV donors can lead to phase instability that in turn accelerates additional photodegradation.[28] However, we hypothesized that varying degrees of intimate mixing of the components in these blends were at least partially responsible for the trends and behavior we observed. Thus, we used photoluminescence quenching measurements in the next section to tease out foundational molecular insights into these phenomenon, and subsequently investigate morphology of several representative blends using scanning tunneling microscopy imaging.

2.2. Time-resolved photoluminescence (TRPL) quenching

Photoluminescence (PL) quenching has previously been used to study polymer–fullerene intercalation,[53] relative fullerene distributions in mixtures of amorphous and semicrystalline polymers,[54] and most recently by us to probe the phase separation of a small molecule donor and $C_{60}(CF_3)_2$ with time during a photobleaching experiment.[28] While we acknowledge that PL quenching is only an indirect measurement of miscibility, stronger PL quenching is generally associated with smaller domains sizes and more intimate mixing,[55] which we contend would help explain the photobleaching data. Here, we performed time-resolved PL measurements to probe the miscibility of each donor and acceptor by comparing the relative degree of PL quenching between $PC_{60}BM$ and $C_{60}(CF_3)_2$ for each polymer. The measurements for a given polymer series were normalized by the number of excitation pulses and then by the fraction of absorbed light at the excitation wavelength (details for each polymer and further discussion are given in the ESI†). PL decays were obtained by integrating the total PL counts over the full PL spectrum and plotting *vs.* time (Fig. 4). The quenching efficiencies were then calculated from the neat and blend PL decays integrated between 0 and 2 ns and are summarized in Table 2.

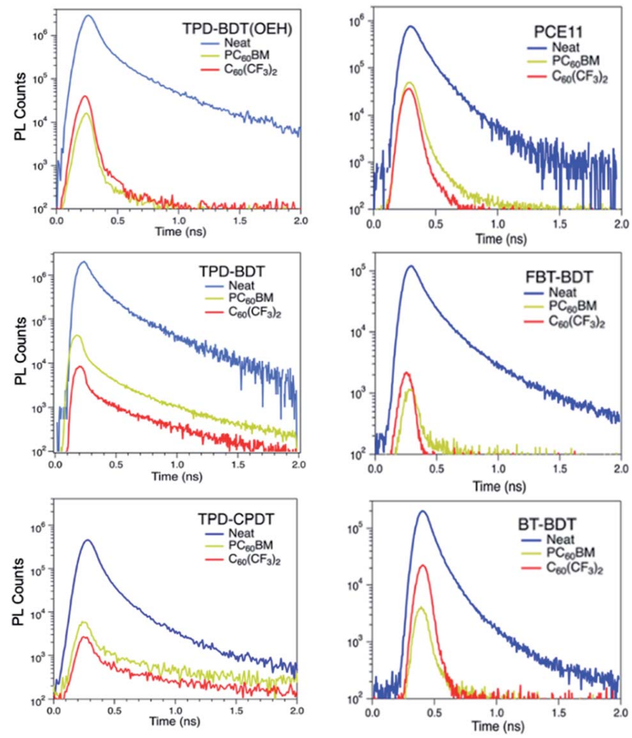

Fig. 4 PL decays for neat and fullerene blends of TPD-BDT(OEH), TPD-BDT, and TPD-CPDT (top, center, and bottom left, respectively), as well as PCE-11, FBT-BDT, and BT-BDT (top, center, and bottom right, respectively). All neat films are represented in blue. Polymer-blends (1 : 1 by mass) with $PC_{60}BM$ and $C_{60}(CF_3)_2$ are coloured orange and red, respectively. TPD-CPDT data was reproduced in part with permission.[56]

We first discuss the quenching efficiencies of the TPD-based polymers shown in Fig. 4, which were all greater than 98% efficient for both $PC_{60}BM$ and $C_{60}(CF_3)_2$. Interestingly, for the TPD-based polymers the stabilization toward photobleaching is correlated with the PL quenching efficiency. For example, in the case of TPD-BDT(OEH), the polymer was more stabilized toward photodegradation by $PC_{60}BM$ than by $C_{60}(CF_3)_2$, and the PL quenching by $PC_{60}BM$ was more efficient for this polymer than by $C_{60}(CF_3)_2$ (99.7 *vs.* 99.2%, respectively). In contrast, the other two TPD polymers were more stabilized by $C_{60}(CF_3)_2$ than by $PC_{60}BM$, and PL quenching by $C_{60}(CF_3)_2$ was more efficient in both cases.

When looking at the other three polymers, a similar trend was observed. The upper right portion of Fig. 4 shows that the

Table 2 Quenching efficiencies (%) with standard deviations

Polymer	$PC_{60}BM$	$C_{60}(CF_3)_2$
TPD-BDT(OEH)	99.7 ± 0.1	99.2 ± 0.3
TPD-BDT	98.4 ± 0.4	99.6 ± 0.4
TPD-CPDT	97.9 ± 0.6	99.2 ± 0.1
BT-BDT	98.4 ± 0.2	92.4 ± 0.7
FBT-BDT	98.5 ± 0.5	98.2 ± 0.5
PCE11	95.6 ± 0.6	97.0 ± 0.4

Published on 25 September 2020. Downloaded by Indian Institute of Science on 12/30/2021 11:43:08 AM.

PL of PCE11 was moderately more efficiently quenched by $C_{60}(CF_3)_2$ compared to $PC_{60}BM$, noting that $C_{60}(CF_3)_2$ had the greater stabilizing effect on this polymer. Moreover, $PC_{60}BM$ was more stabilizing for BT-BDT and was a far more efficient quencher of that polymer's PL. Finally, the data for FBT-BDT might be considered an outlier, as $C_{60}(CF_3)_2$ had the greater stabilizing effect on FBT-BDT while the quenching efficiencies with $C_{60}(CF_3)_2$ was slightly lower (98.2% *vs.* 98.5% with $PC_{60}BM$). However, if we compare the relative quenching data for FBT-BDT and BT-BDT, we see that the substitution of fluorine into the polymer backbone dramatically improved quenching efficiency with $C_{60}(CF_3)_2$, from 92.4 to 98.2%; consistent with the photobleaching results that $C_{60}(CF_3)_2$ had a greater relative stabilizing effect on FBT-BDT than BT-BDT compared to $PC_{60}BM$.

The results for these twelve systems strongly suggest that a full rationalization of the photobleaching data requires consideration of both the electron affinity of the fullerene as well as the relative miscibility of the polymer–fullerene blend. We couple these results with a more direct probe of morphology in the next section.

2.3. Scanning tunneling spectroscopy/microscopy

Scanning tunneling spectroscopy (STS) coupled with scanning tunneling microscopy (STM) is a powerful technique for probing nanoscale morphology in semiconductor materials.[57–60] Indeed, the STS/STM technique has been employed to determine the band edges of nanostructures,[59] to map the band structure in a pn-junction with nanometer resolution,[61] to investigate cross–sectional interfaces in model BHJ OPV systems,[62] and was recently used by us to probe the influence of additives on polymer and fullerene domain size in an OPV active layer.[16] With this technique, transient conductance (dI/dV) images can be used to differentiate semiconductor components based upon their electronic levels and localized density of states (DOS), *i.e.*, polymer and fullerene HOMO and LUMO levels. The materials in a BHJ can therefore be mapped throughout a given sample. Here, we examine bias-dependent localized DOS distributions obtained with tunnel conductance (dI/dV) images for blends of PCE11 and BT-BDT with the two fullerene derivatives. Since these measurements are non-trivial, we opted to down select from twelve polymer–fullerene systems to four (blends with PCE11 and BT-BDT). These particular systems were chosen because (1) they represented the two most stable polymers investigated in this manuscript, and because (2) one polymer (BT-BDT) was more stabilized by $PC_{60}BM$ and the other (PCE11) was more stabilized by $C_{60}(CF_3)_2$.

As the contact and high internal resistances of thick (~100 nm) active layers typically employed in OPV devices is known to skew STS/STM results, we probed the morphologies of ~10 nm thick active layers cast at higher spin speeds from stock solutions of the same concentration as those used for the preparation of blends for photobleaching. The neat films of the polymers were first analyzed by STS at various positions throughout the films in order to ascertain the local DOS and to locate the HOMO and LUMO levels. To obtain a single measurement, the tip was held at a fixed position and sample bias was swept from 2.5 V to −2.5 V while the differential tunnel conductance (dI/dV) spectrum was measured simultaneously using a lock-in amplifier. This allowed us to obtain the dI/dV *versus* voltage plot that would correlate to the nanoscale electronic levels. As the sample is biased in both the negative and positive voltage range, the first peaks nearest to 0 V in both bias directions in the dI/dV spectrum correspond to occupied and unoccupied states, respectively. For neat materials, dI/dV curves afford accurate information regarding the relative positions of HOMO and LUMO energy levels with respect to the Fermi level. For example, Fig. 5 shows histograms of the distributions of local DOS of BT-BDT HOMO and LUMO levels. Each histogram (represented with bars) was compiled from dI/dV spectra from at least 100 different measurements/positions. The STS characteristics of the pure materials then allowed us to distinguish

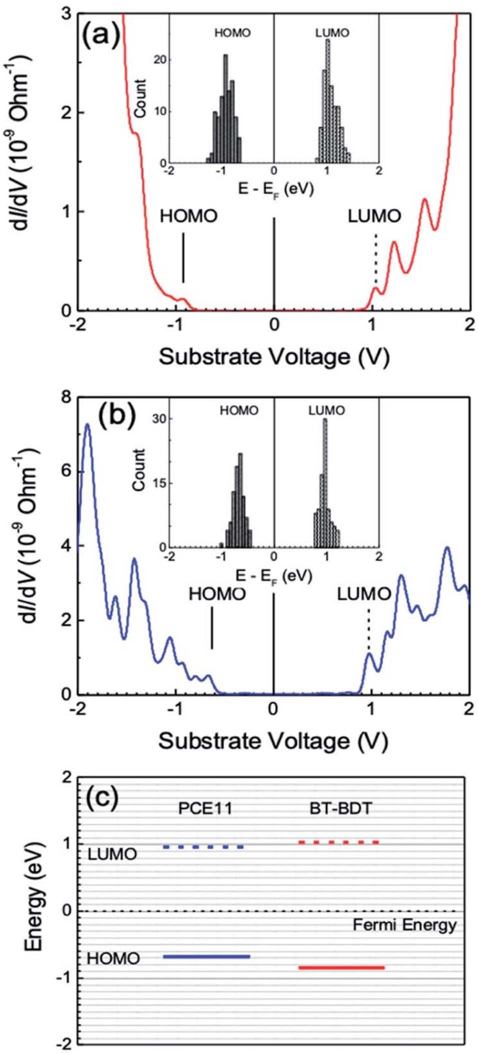

Fig. 5 Differential tunnel conductance (dI/dV) *versus* voltage characteristics of (a) BT-BDT and (b) PCE11 with marked HOMO and LUMO positions and corresponding histograms (inset) of HOMO and LUMO positions obtained from many dI/dV spectra. (c) Energy level diagram of PCE11 and BT-BDT.

 This journal is © The Royal Society of Chemistry 2020

Published on 25 September 2020. Downloaded by Indian Institute of Science on 12/30/2021 11:43:08 AM.

between donor and acceptor components in the blends based on their energy levels. To analyze the d*I*/d*V* images of BHJ's in meaningful manner we need to know the energy levels of at least one component (donor or acceptor) of the BHJ. Fig. 5c represents the energy levels (HOMO and LUMO) of the donor polymers (PCE11 and BT-BDT) of the four selected polymer:-fullerene systems obtained from Fig. 5a and b.

Fig. 6 illustrates STM d*I*/d*V* images corresponding to blends prepared with PCE11 (left) and BT-BDT (right). The data were recorded at a constant sample bias of −0.95 V to view BT-BDT and −0.70 V for PCE11 in the BHJs, selected to specifically probe the HOMO level of the polymers. At these biases, conductance will, by and large, occur through the donor polymer, thus allowing us to visualize the polymer donor domains as brighter (magenta) regions. The green regions in these images represent domains with very low DOS, and hence can be considered fullerene-rich, while the intermediate DOS in the blue regions are likely to represent domains mixed with polymer and fullerene. As we aim to correlate this morphology data with the PL data from the quenching experiments measured in the previous section, we focus our attention and discussion hereafter on the qualitative size and clustering behavior of the polymer (magenta) domains in Fig. 6.

First, we compare differences between two different fullerenes for a given polymer. The image corresponding to the PCE11:$PC_{60}BM$ film in the lower left corner of Fig. 6 suggests that both the polymer and fullerene-rich domains are more clustered in comparison to the PCE11:$C_{60}(CF_3)_2$ film in the upper left corner, where domains are smaller and appear more evenly dispersed. Quantitative analysis of the images reveals that the magenta (polymer rich) regions represent 1.9% of the area of the PCE11:$PC_{60}BM$ images, whereas the polymer-rich regions represent just 1.2% of the area in the PCE11:$C_{60}(CF_3)_2$ images. While those differences are small, the results are consistent with the PL quenching data that indicates $C_{60}(CF_3)_2$ is the more efficient quencher for this polymer. A comparison of the polymer-rich domains in the two BT-BDT images shows the opposite trend; the larger magenta (polymer) domains represent 2.7% of the area in the BT-BDT:$C_{60}(CF_3)_2$ film, compared to just 0.4% in BT-BDT:$PC_{60}BM$. These results are also consistent with the PL quenching efficiencies, as $PC_{60}BM$ was found to be a far more efficient PL quencher than $C_{60}(CF_3)_2$ in films with BT-BDT (98.4% with *vs.* 92.4%, respectively).

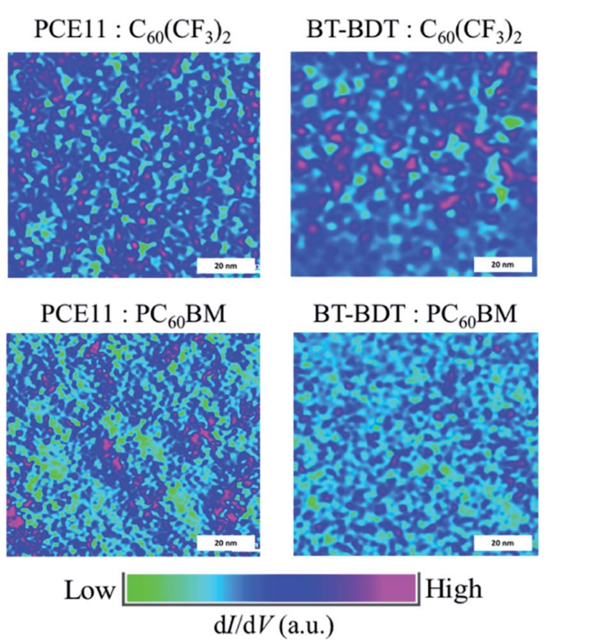

Fig. 6 d*I*/d*V* images corresponding to ~10 nm thick active layer films prepared on Au (111) and imaged under inert atmosphere. Left panel: PCE11. Right panel: BT-BDT. Upper panel: blends with $C_{60}(CF_3)_2$. Lower panel: blends with $PC_{60}BM$. Images were recorded at −0.95 V for BT-BDT and −0.70 V for PCE11, probing the HOMO of the polymers. Hence, magenta regions correspond to polymer donor-rich domains, green to fullerene-rich domains, and blue regions can be considered to represent mixed-domains. White scale bar represents 20 nm.

Next, we compare the difference between the two polymers for a given fullerene. $PC_{60}BM$ quenches the PL of BT-BDT (98.4%) more efficiently than that of PCE11 (95.6%), and as would be anticipated from those data, polymer-rich domains of BT-BDT are smaller (compare magenta spots in the lower two images of Fig. 6). Similarly, $C_{60}(CF_3)_2$ quenches the PL of PCE11 (97.0%) more efficiently than that of BT-BDT (92.4%), and domains of PCE11 are clearly smaller (compare magenta spots in the upper two images of Fig. 6). The STM images are thus fully consistent with the PL quenching data and fully consistent with the photobleaching trends, where $C_{60}(CF_3)_2$ is more efficient at stabilizing PCE11 toward photodegradation, and $PC_{60}BM$ is more efficient at stabilizing BT-BDT. The data further supports our conclusion that a full rationalization of the photobleaching data requires consideration of both the electron affinity of the fullerene as well as the relative miscibility of the polymer–fullerene components in the blend.

2.4. Photoconductance

Time-resolved microwave conductivity (TRMC) is a useful technique for probing and studying photoinduced charge generation in OPV blends.[63–66] Our TRMC setup, along with the general methodology and principles for TRMC, have been thoroughly discussed elsewhere.[67–69] Furthermore, TRMC has recently been used to screen new photovoltaic materials for their potential performance in OPV devices.[42,69–71] Here, we prepared six different samples on quartz substrates, including the neat polymers of PCE11 and BT-BDT along with their blends of $PC_{60}BM$ and $C_{60}(CF_3)_2$, in order to probe the intrinsic photoconductance properties of these materials. The optical density of each film was relatively low (between 0.1 and 0.2 absorbance units), with the films being slightly thinner than those used for the photodegradation experiments. The principal figure-of-merit (the 'yield-mobility product', $\phi\Sigma\mu$), derived from the microwave data is proportional to the product of the sum of the local mobilities ($\Sigma\mu$) of free carriers and the overall yield of free charge carrier generation (ϕ) per absorbed photon.[67] While $\phi\Sigma\mu$ is a complex parameter, the relative miscibility of donor polymers and fullerene acceptors will

Published on 25 September 2020. Downloaded by Indian Institute of Science on 12/30/2021 11:43:08 AM.

necessarily influence the generation of free charge carriers, and we sought to investigate how the TRMC figure of merit might thus be influenced in these different blends.

The TRMC figure of merit was recorded over four orders of excitation intensity, shown in Fig. 7, which allows us to analyze the transition from a regime where higher order processes influence the measured signal towards intensity-independent recombination processes as the excitation intensity is decreased. The $\phi\Sigma\mu$ values at lowest absorbed photon flux of blend films show between one and two orders of magnitude increase relative to the neat polymer, indicating a high yield of free charges per photon absorbed when the acceptor is present. As noted in a previous section, PL quenching in the BT-BDT–$PC_{60}BM$ blend was dramatically more efficient than in the blend with $C_{60}(CF_3)_2$ (98.4 *vs.* 92.1%, respectively). Those PL results appear to correlate with the more pronounced TRMC signal in BT-BDT–$PC_{60}BM$ blends at all excitation intensities, which would be consistent with more efficient exciton dissociation in that blend. For the case of fluorinated PCE11 blended with either $PC_{60}BM$ or $C_{60}(CF_3)_2$, the latter appears to reach the intensity-independent $\phi\Sigma\mu$ regime at almost two orders of magnitude higher in excitation intensity than the former. While the exact origin of this phenomenon is unclear, it may be due to enhanced mixing of the $C_{60}(CF_3)_2$ within PCE11 that in turn favors more exciton to carrier conversion as opposed to higher order exciton quenching processes that can limit ϕ.[72] The fact that the peak $\phi\Sigma\mu$ product is higher at the lowest intensity for the $PC_{60}BM$ blend may be due to a higher electron mobility contribution to the signal compared to $C_{60}(CF_3)_2$.[73]

For both blends of PCE11, the peak $\phi\Sigma\mu$ is amongst the highest values that have been recorded for OPV films in the literature.[42] The BT-BDT polymer blends, on the other hand, are between one and two orders of magnitude lower than the signals for PCE11. The general magnitude of the TRMC figure of merit for both PCE11 and BT-BDT polymers are thus consistent with literature device efficiencies attained for PCE11/$PC_{60}BM$ near 11% (ref. 51) and for derivatives of BT-BDT/$PC_{60}BM$ closer to 3–4%.[52] The fact that the blend of PCE11 with $C_{60}(CF_3)_2$ exhibits a generally comparable response to that with $PC_{60}BM$ in terms of overall magnitude is quite notable. That promising result suggests there is nothing intrinsically limiting in the $C_{60}(CF_3)_2$ blend that would prevent efficient devices from being constructed with this fullerene.

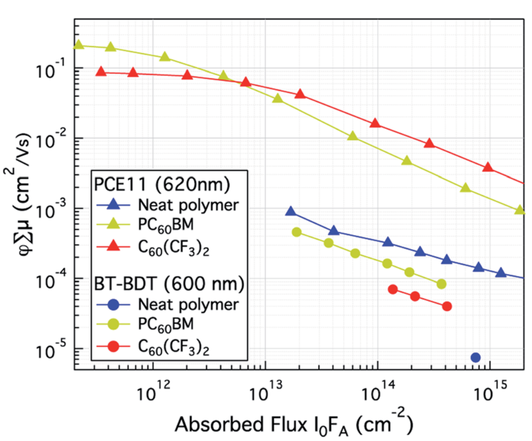

Fig. 7 The product of charge carrier yield (ϕ) and sum of local hole and electron mobilities ($\Sigma\mu$) is illustrated over a range of intensities spanning several orders of magnitude at a laser excitation wavelength of 620 nm for PCE11 samples (triangles) and 600 nm for BT-BDT samples (circles).

That being said, TRMC does not probe differences in open circuit voltages (V_{OC}), which will necessarily be lower for a given polymer in devices with $C_{60}(CF_3)_2$ *vs.* $PC_{60}BM$ as the LUMO of the former is *ca.* 220 mV deeper. While extensive device optimization with $C_{60}(CF_3)_2$ is outside the scope of this manuscript, we do report some preliminary device data in Table S1 of the ESI.† As anticipated, PCE11 devices with $C_{60}(CF_3)_2$ significantly underperform compared to those with $PC_{60}BM$, due in large part to a V_{OC} that is ~290 mV lower with $C_{60}(CF_3)_2$. Nevertheless, the TRMC results suggest that $C_{60}(CF_3)_2$ possesses sufficient intrinsic photoconductance properties to produce high efficiency devices, assuming it is blended with polymers with appropriately deep energy levels to produce high open circuit voltages. Overall, the value of this work does not lay in our ability to demonstrate that $C_{60}(CF_3)_2$ can produce efficient devices with polymers that were developed and optimized for application with $PC_{60}BM$; rather, we envision that the molecular insights regarding electron affinity and polymer–fullerene mixing obtained in this work will provide guidelines for the development of the next generation of fluorinated donor materials with deep energy levels that can be efficiently blended with $C_{60}(CF_3)_2$ and higher trifluoromethyl fullerenes for enhanced photostability.

3. Conclusions

While so much of the literature focus in the field of OPV over the last decade has revolved around improving device efficiencies, this work advances the state of OPV science by providing molecular insight and foundational understanding around the photostability of OPV donor–acceptor blends. We demonstrated that rationalizing complex photobleaching behaviour ultimately required consideration of the electron affinity of the fullerene *as well as* the relative miscibility of the polymer–fullerene blend. The ability of $C_{60}(CF_3)_2$ to stabilize certain donor materials towards photodegradation, to blend well with fluorinated (and even certain non-fluorinated) polymers, and to quench excited states efficiently were all thoroughly demonstrated and correlated with structure–property relationships amongst several polymer donor and fullerene acceptor combinations in this manuscript. We believe the methodology and guiding principles in this work set the stage for a new paradigm in OPV materials development, including the design of more intrinsically oxidatively stable donor materials whose LUMO levels are otherwise too deep to work in conjunction with $PC_{60}BM$ or other traditional acceptors in an OPV device, but whose energetics would make $C_{60}(CF_3)_2$, other fluorinated fullerenes,[30] or fluorinated small molecule acceptors[74] more optimal substitutes.

Published on 25 September 2020. Downloaded by Indian Institute of Science on 12/30/2021 11:43:08 AM.

Conflicts of interest

There are no conflicts to declare.

Acknowledgements

This work was authored in part by Alliance for Sustainable Energy, LLC, the manager and operator of the National Renewable Energy Laboratory for the U.S. Department of Energy (DOE) under contract no. DE-AC36-08GO28308. Project conception, photobleaching studies, TRPL, and device work were supported by the Solar Energy Research Institute for India and the US funded jointly by the U.S. Department of Energy (Office of Science, Office of Basic Energy Sciences, and Energy Efficiency and Renewable Energy, Solar Energy Technology Office, with support from the Office of International Affairs) and the Government of India subcontract IUSSTF/JCERDCSERIIUS/2012 dated 22nd Nov. 2012. TRMC measurements and analysis were performed by B. W. L. and A. J. F. and supported through a separate grant from the U.S. Department of Energy with the National Renewable Energy Laboratory through the Office of Energy Efficiency and Renewable Energy, Solar Energy Technologies Office. S. S. and O. B. acknowledge support from NSF Grant CHEM-1362302 for synthesis and characterization of $C_{60}(CF_3)_2$. A. J. P. acknowledges the JC Bose National Fellowship (SB/S2/JCB-001/2016) of SERB and G. P. acknowledges the CSIR Junior Research Fellowship Number 09/080(1042)/2017-EMR-I (roll no. 523509) for STS/STM measurements and analysis. The views expressed in the article do not necessarily represent the views of the DOE or the U.S. Government. The U.S. Government retains and the publisher, by accepting the article for publication, acknowledges that the U.S. Government retains a nonexclusive, paid-up, irrevocable, worldwide license to publish or reproduce the published form of this work, or allow others to do so, for U.S. Government purposes.

Notes and references

1 T. R. Andersen, H. F. Dam, M. Hosel, M. Helgesen, J. E. Carle, T. T. Larsen-Olsen, S. A. Gevorgyan, J. W. Andreasen, J. Adams, N. Li, F. Machui, G. D. Spyropoulos, T. Ameri, N. Lemaitre, M. Legros, A. Scheel, D. Gaiser, K. Kreul, S. Berny, O. R. Lozman, S. Nordman, M. Valimaki, M. Vilkman, R. R. Sondergaard, M. Jorgensen, C. J. Brabec and F. C. Krebs, *Energy Environ. Sci.*, 2014, **7**, 2925–2933.

2 F. C. Krebs, N. Espinosa, M. Hösel, R. R. Søndergaard and M. Jørgensen, *Adv. Mater.*, 2014, **26**, 29–39.

3 A. Wadsworth, R. S. Ashraf, M. Abdelsamie, S. Pont, M. Little, M. Moser, Z. Hamid, M. Neophytou, W. Zhang, A. Amassian, J. R. Durrant, D. Baran and I. McCulloch, *ACS Energy Lett.*, 2017, **2**, 1494–1500.

4 D. Deng, Y. Zhang, J. Zhang, Z. Wang, L. Zhu, J. Fang, B. Xia, Z. Wang, K. Lu, W. Ma and Z. Wei, *Nat. Commun.*, 2016, **7**, 13740.

5 W. Zhao, S. Li, H. Yao, S. Zhang, Y. Zhang, B. Yang and J. Hou, *J. Am. Chem. Soc.*, 2017, **139**, 7148–7151.

6 Y. Lin, B. Adilbekova, Y. Firdaus, E. Yengel, H. Faber, M. Sajjad, X. Zheng, E. Yarali, A. Seitkhan, O. M. Bakr, A. El-Labban, U. Schwingenschloegl, V. Tung, I. McCulloch, F. Laquai and T. D. Anthopoulos, *Adv. Mater.*, 2019, **31**, 1902965.

7 Y. Cui, H. Yao, L. Hong, T. Zhang, Y. Tang, B. Lin, K. Xian, B. Gao, C. An, P. Bi, W. Ma and J. Hou, *Natl. Sci. Rev.*, 2020, **7**, 1239–1246.

8 L. Meng, Y. Zhang, X. Wan, C. Li, X. Zhang, Y. Wang, X. Ke, Z. Xiao, L. Ding, R. Xia, H.-L. Yip, Y. Cao and Y. Chen, *Science*, 2018, **361**, 1094–1098.

9 H. Kang, G. Kim, J. Kim, S. Kwon, H. Kim and K. Lee, *Adv. Mater.*, 2016, **28**, 7821–7861.

10 W. R. Mateker, I. T. Sachs-Quintana, G. F. Burkhard, R. Cheacharoen and M. D. McGehee, *Chem. Mater.*, 2015, **27**, 404–407.

11 J. Adams, G. D. Spyropoulos, M. Salvador, N. Li, S. Strohm, L. Lucera, S. Langner, F. Machui, H. Zhang, T. Ameri, M. M. Voigt, F. C. Krebs and C. J. Brabec, *Energy Environ. Sci.*, 2015, **8**, 169–176.

12 W. R. Mateker and M. D. McGehee, *Adv. Mater.*, 2017, **29**, 1603940.

13 M. Jørgensen, K. Norrman, S. A. Gevorgyan, T. Tromholt, B. Andreasen and F. C. Krebs, *Adv. Mater.*, 2012, **24**, 580–612.

14 N. Grossiord, J. M. Kroon, R. Andriessen and P. W. M. Blom, *Org. Electron.*, 2012, **13**, 432–456.

15 W. R. Mateker, J. D. Douglas, C. Cabanetos, I. T. Sachs-Quintana, J. A. Bartelt, E. T. Hoke, A. El Labban, P. M. Beaujuge, J. M. J. Frechet and M. D. McGehee, *Energy Environ. Sci.*, 2013, **6**, 2529–2537.

16 L. E. Garner, A. Bera, B. W. Larson, D. P. Ostrowski, A. J. Pal and W. A. Braunecker, *ACS Energy Lett.*, 2017, **2**, 1556–1563.

17 N. Li, J. D. Perea, T. Kassar, M. Richter, T. Heumueller, G. J. Matt, Y. Hou, N. S. Güldal, H. Chen, S. Chen, S. Langner, M. Berlinghof, T. Unruh and C. J. Brabec, *Nat. Commun.*, 2017, **8**, 14541.

18 C. Muller, J. Bergqvist, K. Vandewal, K. Tvingstedt, A. S. Anselmo, R. Magnusson, M. I. Alonso, E. Moons, H. Arwin, M. Campoy-Quiles and O. Inganas, *J. Mater. Chem.*, 2011, **21**, 10676–10684.

19 N. D. Treat, A. Varotto, C. J. Takacs, N. Batara, M. Al-Hashimi, M. J. Heeney, A. J. Heeger, F. Wudl, C. J. Hawker and M. L. Chabinyc, *J. Am. Chem. Soc.*, 2012, **134**, 15869–15879.

20 L. Ye, H. Hu, M. Ghasemi, T. Wang, B. A. Collins, J.-H. Kim, K. Jiang, J. H. Carpenter, H. Li, Z. Li, T. McAfee, J. Zhao, X. Chen, J. L. Y. Lai, T. Ma, J.-L. Bredas, H. Yan and H. Ade, *Nat. Mater.*, 2018, **17**, 253–260.

21 L. Ye, B. A. Collins, X. Jiao, J. Zhao, H. Yan and H. Ade, *Adv. Energy Mater.*, 2018, **8**, 1703058.

22 E. T. Hoke, I. T. Sachs-Quintana, M. T. Lloyd, I. Kauvar, W. R. Mateker, A. M. Nardes, C. H. Peters, N. Kopidakis and M. D. McGehee, *Adv. Energy Mater.*, 2012, **2**, 1351–1357.

23 M. C. Carvalho de Oliveira, A. S. A. D. Cardoso, M. M. Viana and V. d. F. C. Lins, *Renewable Sustainable Energy Rev.*, 2018, **81**, 2299–2317.

Published on 25 September 2020. Downloaded by Indian Institute of Science on 12/30/2021 11:43:08 AM.

24 H. Hintz, H. J. Egelhaaf, H. Peisert and T. Chassé, *Polym. Degrad. Stab.*, 2010, **95**, 818–825.

25 A. Tournebize, P.-O. Bussière, A. Rivaton, J.-L. Gardette, H. Medlej, R. C. Hiorns, C. Dagron-Lartigau, F. C. Krebs and K. Norrman, *Chem. Mater.*, 2013, **25**, 4522–4528.

26 L. K. San, E. V. Bukovsky, B. W. Larson, J. B. Whitaker, S. H. M. Deng, N. Kopidakis, G. Rumbles, A. A. Popov, Y.-S. Chen, X.-B. Wang, O. V. Boltalina and S. H. Strauss, *Chem. Sci.*, 2015, **6**, 1801–1815.

27 A. A. Popov, I. E. Kareev, N. B. Shustova, E. B. Stukalin, S. F. Lebedkin, K. Seppelt, S. H. Strauss, O. V. Boltalina and L. Dunsch, *J. Am. Chem. Soc.*, 2007, **129**, 11551–11568.

28 L. E. Garner, V. Nellissery Viswanathan, D. H. Arias, C. P. Brook, S. T. Christensen, A. J. Ferguson, N. Kopidakis, B. W. Larson, Z. R. Owczarczyk, J. R. Pfeilsticker, P. C. Ramamurthy, S. H. Strauss, O. V. Boltalina and W. A. Braunecker, *J. Mater. Chem. A*, 2018, **6**, 4623–4628.

29 V. Nellissery Viswanathan, A. J. Ferguson, J. R. Pfeilsticker, B. W. Larson, L. E. Garner, C. P. Brook, S. H. Strauss, O. V. Boltalina, P. C. Ramamurthy and W. A. Braunecker, *Org. Electron.*, 2018, **62**, 685–694.

30 O. V. Boltalina, A. A. Popov, I. V. Kuvychko, N. B. Shustova and S. H. Strauss, *Chem. Rev.*, 2015, **115**, 1051–1105.

31 C. Zhang, S. Langner, A. V. Mumyatov, D. V. Anokhin, J. Min, J. D. Perea, K. L. Gerasimov, A. Osvet, D. A. Ivanov, P. Troshin, N. Li and C. J. Brabec, *J. Mater. Chem. A*, 2017, **5**, 17570–17579.

32 W. Huang, E. Gann, N. Chandrasekaran, S. K. K. Prasad, S.-Y. Chang, L. Thomsen, D. Kabra, J. M. Hodgkiss, Y.-B. Cheng, Y. Yang and C. R. McNeill, *Adv. Energy Mater.*, 2017, **7**, 1602197.

33 G. Han, Y. Guo, R. Duan, X. Shen and Y. Yi, *J. Mater. Chem. A*, 2017, **5**, 9316–9321.

34 Q. Zhang, L. Yan, X. Jiao, Z. Peng, S. Liu, J. J. Rech, E. Klump, H. Ade, F. So and W. You, *Chem. Mater.*, 2017, **29**, 5990–6002.

35 N. Bauer, Q. Zhang, J. Zhu, Z. Peng, L. Yan, C. Zhu, H. Ade, X. Zhan and W. You, *J. Mater. Chem. A*, 2017, **5**, 22536–22541.

36 V. N. Viswanathan, A. D. Rao, U. K. Pandey, A. V. Kesavan and P. C. Ramamurthy, *Beilstein J. Org. Chem.*, 2017, **13**, 863–873.

37 C. L. Chochos, N. Leclerc, N. Gasparini, N. Zimmermann, E. Tatsi, A. Katsouras, D. Moschovas, E. Serpetzoglou, I. Konidakis, S. Fall, P. Leveque, T. Heiser, M. Spanos, V. G. Gregoriou, E. Stratakis, T. Ameri, C. J. Brabec and A. Avgeropoulos, *J. Mater. Chem. A*, 2017, **5**, 25064–25076.

38 J. Yuan, M. J. Ford, Y. Zhang, H. Dong, Z. Li, Y. Li, T.-Q. Nguyen, G. C. Bazan and W. Ma, *Chem. Mater.*, 2017, **29**, 1758–1768.

39 A. C. Stuart, J. R. Tumbleston, H. Zhou, W. Li, S. Liu, H. Ade and W. You, *J. Am. Chem. Soc.*, 2013, **135**, 1806–1815.

40 K. Reichenbacher, H. I. Suss and J. Hulliger, *Chem. Soc. Rev.*, 2005, **34**, 22–30.

41 T. Heumueller, W. R. Mateker, I. T. Sachs-Quintana, K. Vandewal, J. A. Bartelt, T. M. Burke, T. Ameri, C. J. Brabec and M. D. McGehee, *Energy Environ. Sci.*, 2014, **7**, 2974–2980.

42 S. D. Oosterhout, N. Kopidakis, Z. R. Owczarczyk, W. A. Braunecker, R. E. Larsen, E. L. Ratcliff and D. C. Olson, *J. Mater. Chem. A*, 2015, **3**, 9777–9788.

43 L. Lu and L. Yu, *Adv. Mater.*, 2014, **26**, 4413–4430.

44 R. Berger, G. Resnati, P. Metrangolo, E. Weber and J. Hulliger, *Chem. Soc. Rev.*, 2011, **40**, 3496–3508.

45 H. Sun, U. K. Tottempudi, J. D. Mottishaw, P. N. Basa, A. Putta and A. G. Sykes, *Cryst. Growth Des.*, 2012, **12**, 5655–5662.

46 H. Omorodion, B. Twamley, J. A. Platts and R. J. Baker, *Cryst. Growth Des.*, 2015, **15**, 2835–2841.

47 W. A. Braunecker, K. E. Hurst, K. G. Ray, Z. R. Owczarczyk, M. B. Martinez, N. Leick, A. Keuhlen, A. Sellinger and J. C. Johnson, *Cryst. Growth Des.*, 2018, **18**, 4160–4166.

48 H. Yao, L. Ye, H. Zhang, S. Li, S. Zhang and J. Hou, *Chem. Rev.*, 2016, **116**, 7397–7457.

49 Z. Li, S.-W. Tsang, X. Du, L. Scoles, G. Robertson, Y. Zhang, F. Toll, Y. Tao, J. Lu and J. Ding, *Adv. Funct. Mater.*, 2011, **21**, 3331–3336.

50 C. Cabanetos, A. El Labban, J. A. Bartelt, J. D. Douglas, W. R. Mateker, J. M. J. Frechet, M. D. McGehee and P. M. Beaujuge, *J. Am. Chem. Soc.*, 2013, **135**, 4656–4659.

51 Y. Liu, J. Zhao, Z. Li, C. Mu, W. Ma, H. Hu, K. Jiang, H. Lin, H. Ade and H. Yan, *Nat. Commun.*, 2014, **5**, 5293.

52 C. Gao, L. Wang, X. Li and H. Wang, *Polym. Chem.*, 2014, **5**, 5200–5210.

53 W. L. Rance, A. J. Ferguson, T. McCarthy-Ward, M. Heeney, D. S. Ginley, D. C. Olson, G. Rumbles and N. Kopidakis, *ACS Nano*, 2011, **5**, 5635–5646.

54 M. T. Sajjad, A. J. Ward, C. Kästner, A. Ruseckas, H. Hoppe and I. D. W. Samuel, *J. Phys. Chem. Lett.*, 2015, **6**, 3054–3060.

55 X. Yi, Z. Peng, B. Xu, D. Seyitliyev, C. H. Y. Ho, E. O. Danilov, T. Kim, J. R. Reynolds, A. Amassian, K. Gundogdu, H. Ade and F. So, *Adv. Energy Mater.*, 2020, **10**, 1902430.

56 Reprinted from Org. Electron., 62, V. Nellissery Viswanathan, A. J. Ferguson, J. R. Pfeilsticker, B. W. Larson, L. E. Garner, C. P. Brook, S. H. Strauss, O. V. Boltalina, P. C. Ramamurthy and W. A. Braunecker, *Strategic fluorination of polymers and fullerenes improves photostability of organic photovoltaic blends*, 2018, pp. 685–694, with permission from Elsevier.

57 U. Banin, Y. Cao, D. Katz and O. Millo, *Nature*, 1999, **400**, 542–544.

58 L. Wang, Q. Chen, G. B. Pan, L. J. Wan, S. Zhang, X. Zhan, B. H. Northrop and P. J. Stang, *J. Am. Chem. Soc.*, 2008, **130**, 13433–13441.

59 D. Mocatta, G. Cohen, J. Schattner, O. Millo, E. Rabani and U. Banin, *Science*, 2011, **332**, 77–81.

60 T. Y. Chien, L. F. Kourkoutis, J. Chakhalian, B. Gray, M. Kareev, N. P. Guisinger, D. A. Muller and J. W. Freeland, *Nat. Commun.*, 2013, **4**, 2336.

61 A. Bera, S. Dey and A. J. Pal, *Nano Lett.*, 2014, **14**, 2000–2005.

62 M. C. Shih, B. C. Huang, C. C. Lin, S. S. Li, H. A. Chen, Y. P. Chiu and C. W. Chen, *Nano Lett.*, 2013, **13**, 2387–2392.

63 W. A. Braunecker, Z. R. Owczarczyk, A. Garcia, N. Kopidakis, R. E. Larsen, S. R. Hammond, D. S. Ginley and D. C. Olson, *Chem. Mater.*, 2012, **24**, 1346–1356.

 This journal is © The Royal Society of Chemistry 2020

Published on 25 September 2020. Downloaded by Indian Institute of Science on 12/30/2021 11:43:08 AM.

64 W. A. Braunecker, S. D. Oosterhout, Z. R. Owczarczyk, R. E. Larsen, B. W. Larson, D. S. Ginley, O. V. Boltalina, S. H. Strauss, N. Kopidakis and D. C. Olson, *Macromolecules*, 2013, **46**, 3367–3375.

65 W. A. Braunecker, S. D. Oosterhout, Z. R. Owczarczyk, N. Kopidakis, E. L. Ratcliff, D. S. Ginley and D. C. Olson, *ACS Macro Lett.*, 2014, **3**, 622–627.

66 S. D. Oosterhout, W. A. Braunecker, Z. R. Owczarczyk, A. L. Ayzner, M. F. Toney, D. C. Olson and N. Kopidakis, *Org. Electron.*, 2017, **47**, 57–65.

67 A. J. Ferguson, N. Kopidakis, S. E. Shaheen and G. Rumbles, *J. Phys. Chem. C*, 2011, **115**, 23134–23148.

68 S. Dayal, N. Kopidakis and G. Rumbles, *Faraday Discuss.*, 2012, **155**, 323–337.

69 T. J. Savenije, A. J. Ferguson, N. Kopidakis and G. Rumbles, *J. Phys. Chem. C*, 2013, **117**, 24085–24103.

70 Z. R. Owczarczyk, W. A. Braunecker, S. D. Oosterhout, N. Kopidakis, R. E. Larsen, D. S. Ginley and D. C. Olson, *Adv. Energy Mater.*, 2014, **4**, 1301821.

71 A. Saeki, S. Yoshikawa, M. Tsuji, Y. Koizumi, M. Ide, C. Vijayakumar and S. Seki, *J. Am. Chem. Soc.*, 2012, **134**, 19035–19042.

72 A. J. Ferguson, N. Kopidakis, S. E. Shaheen and G. Rumbles, *J. Phys. Chem. C*, 2008, **112**, 9865–9871.

73 B. W. Larson, O. G. Reid, D. C. Coffey, S. M. Avdoshenko, A. A. Popov, O. V. Boltalina, S. H. Strauss, N. Kopidakis and G. Rumbles, *Adv. Energy Mater.*, 2016, **6**, 1601427.

74 T. J. Aldrich, M. Matta, W. Zhu, S. M. Swick, C. L. Stern, G. C. Schatz, A. Facchetti, F. S. Melkonyan and T. J. Marks, *J. Am. Chem. Soc.*, 2019, **141**, 3274–3287.

This journal is © The Royal Society of Chemistry 2020